AIMS Mathematics, 8(10): 23578–23602.
DOI: 10.3934/math.20231199
Received: 10 May 2023
Revised: 17 June 2023
Accepted: 30 June 2023
Published: 31 July 2023

http://www.aimspress.com/journal/Math

Research article

The influence of an appropriate reporting time and publicity intensity on the spread of infectious diseases

Chang Hou and Qiubao Wang*

Department of Mathematical and Physics, Shijiazhuang Tiedao University, Shijiazhuang 050043, China

* **Correspondence:** Email: wangqiubao12@sina.com.

Abstract: We present a stochastic time-delay susceptible-exposed-asymptomatic-symptom-vaccinated-recovered (SEAQVR) model with media publicity effect in this study. The model takes into account the impacts of noise, time delay and public sensitivity on infectious illness propagation. The stochastic dynamics of the system are analyzed at the Hopf bifurcation, using time delay and noise intensity as bifurcation parameters, and the theoretical conclusions are validated using numerical simulation. Increasing the time delay and sensitivity coefficient can effectively delay the occurrence of the peak number of infected individuals and mitigate the extent of infection. Additionally, time delay and noise intensity are shown to have specific thresholds, beyond which periodic infections occur. Notably, heightened public sensitivity reduces the threshold for time delay, and media publicity directly affects public sensitivity. The numerical simulation reveals that increasing media publicity intensity does not always yield better results, and that the sensitivity of the public at present is an important reference index for setting an appropriate publicity intensity.

Keywords: noise; time delay; SEAQVR model; sensitivity coefficient; Hopf bifurcation
Mathematics Subject Classification: 37H20, 37N25

1. Introduction

In recent years, the dynamics of infectious diseases have changed fundamentally as a result of population increase, faster urbanization, climate change and economic globalization. Particularly, people have become more prone to infectious illness epidemics, and particular microbes have gained medication resistance. We have also discovered substantial changes in vector ecology, such as increased Aedes activity, which leads to increased disease dissemination. Furthermore, because of modern society's high degree of connectedness and urbanization, diseases are more prone to spread among people [1]. Dengue fever broke out globally in 2016, resulting in 100 million illnesses

and 38,000 deaths [2]. When an infectious disease spreads, it not only harms people's bodily and mental health, but it also necessitates the use of human, material and financial resources to manage it. In some developing countries, serious infectious diseases will generate civil discontent and impede social development. As a result, analyzing the transmission trend of infectious diseases and controlling measures is critical.

In 1972, Kermack and McKendrick constructed the SIR cabin model [3] by using the dynamic system modeling method, which divided the population into three types and studied the disease's spread law and epidemic mechanism in detail, laying the theoretical foundation for the dynamic model of infectious diseases. In recent years, Korolev developed an SEIRD model which outlines how to use supplementary information from random tests to calibrate the model's initial parameters and restrict the range of probable forecasts for future deaths [4]. The SEAIR model was developed by Basnarkov, who discovered that the centrality of feature vectors roughly determines the chance of infection [5]. He et al. proposed a fractional discrete-time SIR model with vaccination, which proved and quantified the complex dynamics of the system [6]. Meng et al. developed the SEIRV model and an evolutionary game model to investigate the differences between forced and voluntary inoculation methods in heterogeneous networks [7]. Goel developed an SIR model with a Holling type-II treatment rate and used the Lyapunov approach to investigate the stability of the equilibrium point [8].

The media is crucial in the prevention and control of infectious diseases [9]. When an epidemic spreads in a country, the government employs the media to educate citizens on how to appropriately respond. The execution of certain policies and the dissemination of information will have an impact on human behavior [10, 11]. Public preventative measures that are implemented on time and effectively can significantly reduce the infection rate [12]. The intensities of publicity, cultural level and social duty may influence people's sensitivity to information published in the media [13, 14]. Individualism, collectivism and ethnic diversity will each have an impact on how people respond to health emergencies [15].

Examining the impact of time delay on system stability constitutes a crucial aspect of investigating system dynamics. Studying the epidemic model with time delay can better depict the transmission mechanism of illnesses because most biological processes involve time delay. Misra et al. analyzed the stability and direction of the Hopf bifurcation, as well as the time delay of carrying out an awareness plan [16]. According to Gutierrez et al., a delay in reporting the death toll resulted in a significant increase in illness severity [17]. The public's behavior and psychological state will be impacted by the media's delayed reporting of the pandemic scenario, which is also influenced by technology, capability, resources and other variables.

Random factors strongly impact the propagation of infectious illnesses in nature. Factors such as immunity, temperature and humidity, for example, will affect the infection rate. People will take different countermeasures based on the heterogeneity of information, which will interfere with the infection rate. The deterministic equation has been idealized. In comparison to the deterministic equation, the stochastic equation can more accurately represent the actual scenario [18–23]. According to the Din et al. stochastic model, noise assured the extinction of the hepatitis B virus [24]. Krause et al. extended the random SIS epidemic model to the spatial network, thus obtaining the random epidemic ensemble population model; they discovered that Gaussian white noise can be used to offset the cure rate [25]. These random factors can be approximately simulated by Gaussian white noise and introduced into the deterministic epidemic model to study the influence of noise on the dynamic

behavior of the system [26].

Based on the model presented in [27], this paper examines the influence of reporting time delay and Gaussian white noise on infection rates. It introduces the sensitivity coefficient, denoted as "k," which represents the public's responsiveness to the number of newly infected individuals displaying symptoms. A stochastic differential equation model incorporating time delay is developed. Excessive promotion or non-dissemination of information about infectious diseases is generally not recommended. By conducting dynamic analyses of time delay, noise intensity and the sensitivity coefficient, this research provides valuable insights for media organizations to devise appropriate publicity strategies. Numerical simulations were performed to investigate the impact of different levels of public sensitivity on the selection of effective publicity intensity.

This paper is structured as follows: In the second section, we provide a detailed explanation of the SEAVQR model, the calculation of the basic reproductive number and the necessary conditions for the existence of the endemic equilibrium point. We further investigate the Hopf bifurcation conditions and present the stability analysis. The third section focuses on deriving the stochastic Itô equation and examining the occurrence of stochastic bifurcation. In the fourth section, we discuss the numerical simulation to analyze the respective influences of reporting time delay, the sensitivity coefficient and noise intensity on the spread of infectious diseases. Finally, in the fifth part, we summarize the findings from the preceding sections.

2. The analysis of the model

Building upon the model proposed in [27], we consider the effects of noise, reporting time delay and the sensitivity coefficient on the infection rate β, and introduce the SEAQVR model. Figure 1 illustrates the schematic diagram of the model, while the model itself is described as follows:

$$\begin{aligned}
&\frac{dS}{dt} = (1-\eta)\Omega + \Gamma V - \frac{\beta AS}{N} - \mu S,\\
&\frac{dE}{dt} = \frac{\beta AS}{N} + \frac{\beta_g AV}{N} - (\varphi+\mu)E,\\
&\frac{dA}{dt} = \alpha\varphi E - (\rho+\mu+\delta)A,\\
&\frac{dQ}{dt} = (1-\alpha)\varphi E - (\gamma+\mu+\delta)Q,\\
&\frac{dV}{dt} = \eta\Omega - \frac{\beta_g AV}{N} - (\Gamma+\mu)V,\\
&\frac{dR}{dt} = \rho A + \gamma Q - \mu R,\\
&\beta(k,\tau,t) = \frac{\beta_0}{1+\left(k+\varepsilon^{\frac{1}{2}}\xi(t)\right)\arctan\left(Q(t)-Q(t-\tau)\right)}.
\end{aligned} \tag{2.1}$$

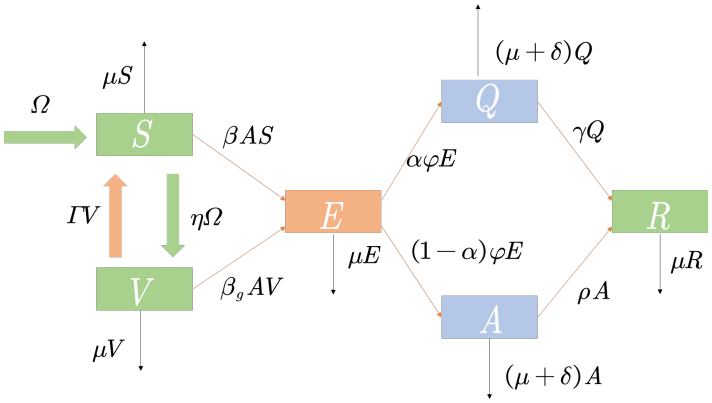

Figure 1. Model schematic diagram.

Population has been divided into six categories: susceptible (S), exposed (E), asymptomatic infected (A), symptomatic infected (Q), vaccinated (V) and recovered (R). Ω denotes the supplementary population, μ represents the natural mortality rate, δ signifies the mortality rate, φ denotes the rate of transition from exposed individuals to infected individuals and γ refers to the recovery rate of infected individuals, both symptomatic and asymptomatic. η denotes the vaccination rate, while Γ represents the rate of vaccine failure. α represents the proportion of symptomatic individuals among the infected population, whereas β and β_g denote the infection rates post-vaccination and without vaccination, respectively. We posit that β is influenced by the collective awareness of prevention among the general public. As the number of infections escalates, individuals often proactively adopt measures to safeguard themselves and impede the transmission chain, while also bolstering their own immunity. k is the coefficient of sensitivity of the public to the number of new symptomatic infections. Naturally, the level of protection corresponds to the sensitivity of the public. The greater the sensitivity, the more active and vigilant are the protective measures. However, in real-world situations, the public's sensitivity to the number of newly infected individuals varies. For instance, if the public lacks accurate information, society becomes permeated with feelings of fear and confusion, consequently disrupting the public's sensitivity. With a range of $\left(-\frac{\pi}{2}, \frac{\pi}{2}\right)$, $\arctan x$ is a monotonically increasing odd function with a flat change and global boundedness. The model becomes more logical because it can adjust the infection rate β within $(0, 1)$. $\xi(t)$ is Gaussian white noise with a power spectral density, and ε is a sufficiently small-scale parameter.

The basic reproductive number R_0 represents the average number of infections in a susceptible population for an infected person in a disturbance-free system. There is always a disease-free equilibrium point $P_1(S_1, E_1, A_1, Q_1, V_1, R_1)$ in the system, where $S_1 = \frac{\Omega(\Gamma+\mu(1-\eta))}{\mu(\mu+\Gamma)}$, $V_1 = \frac{\eta\Omega}{\Gamma+\mu}$ and $E_1 = A_1 = Q_1 = R_1 = 0$. The basic reproductive number of the undisturbed model, as calculated via the next-generation matrix method [28], is

$$R_0 = \frac{\Omega\varphi\alpha\left(\eta\mu\left(\beta_g - \beta_0\right) + \beta_0(\mu+\Gamma)\right)}{\mu N(\mu+\Gamma)(\mu+\rho+\delta)(\varphi+\mu)}.$$

Next, the dynamic behavior near the endemic equilibrium point is considered.

Theorem 2.1. *If $R_0 > 1$, system (2.1) has an endemic equilibrium. If $R_0 < 1$, system (2.1) has no endemic equilibrium.*

Proof. Assuming that the right-hand term of the first six equations in (2.1) are equal to 0, we can determine the endemic equilibrium point $P^*(S^*, E^*, A^*, Q^*, V^*, R^*)$, where

$$\begin{aligned} S^* &= \frac{N(1-\eta)\Omega}{\beta_0 A^* + \mu N} + \frac{\Gamma\eta\Omega N^2}{(\beta_0 A^* + \mu N)\left(\beta_g A^* + \Gamma N + \mu N\right)}, \\ E^* &= \frac{\rho+\mu+\delta}{\alpha\varphi} A^*, \\ V^* &= \frac{\eta\Omega N}{\beta_g A^* + \Gamma N + \mu N}, \\ Q^* &= \frac{(1-\alpha)(\rho+\mu+\delta)}{(\gamma+\mu+\delta)\alpha} A^*, \\ R^* &= \left(\frac{\rho}{\mu} + \frac{\gamma(1-\alpha)(\rho+\mu+\delta)}{\mu\alpha(\gamma+\mu+\delta)}\right) A^*. \end{aligned}$$

A^* satisfies the following equation:

$$D(A^*) = m_1 A^{*2} + m_2 A^* + m_3 = 0, \tag{2.2}$$

where

$m_1 = -\beta_0 N\beta_g(\mu+\varphi)(\delta+\mu+\rho)$

$m_2 = \alpha\beta_0 N\varphi\Omega\beta_g - \mu N^2\beta_g(\mu+\varphi)(\delta+\mu+\rho) - \beta_0 N^2(\Gamma+\mu)(\mu+\varphi)(\delta+\mu+\rho)$

$m_3 = \alpha\eta\mu N^2\varphi\Omega\beta_g + \alpha\beta_0 N^2\varphi\Omega(\Gamma - \eta\mu + \mu) - \mu N^3(\Gamma+\mu)(\mu+\varphi)(\delta+\mu+\rho)$.

Clearly, considering the condition $m_1 < 0$, let us assume that A_1 and A_2 represent two roots of (2.2). If the condition $R_0 > 1$ is met, we have that $m_3 > 0$. Then, $A_1 A_2 < 0$ is obtained, indicating the existence of a positive root among the two roots, and, consequently, an endemic equilibrium point. □

In the case of $R_0 < 1$, $m_3 < 0$. So, we have that $A_1 A_2 > 0$, indicating that both roots can be either positive or negative. In this scenario, the following formula holds.

$$\begin{aligned} m_2 &= \alpha\beta_0 N\varphi\Omega\beta_g - \mu N^2\beta_g(\mu+\varphi)(\delta+\mu+\rho) - \beta_0 N^2(\Gamma+\mu)(\mu+\varphi)(\delta+\mu+\rho) \\ &< \frac{1}{(\Gamma+\mu)N}\left(\alpha\eta\mu\varphi\Omega\left(\beta_0 - \beta_g\right) - \frac{\beta_0}{\beta_g} N(\Gamma+\mu)^2(\mu+\varphi)(\delta+\mu+\rho)\right) \\ &< 0. \end{aligned}$$

Consequently, $A_1 + A_2 < 0$, indicating that both roots are negative and there is no existence of an endemic equilibrium point.

Considering that the first five equations of (2.1) do not account for the recovered individuals (R), the following only analyzes the first five equations and linearizes the system at the endemic equilibrium point. Let $\varepsilon x_1 = S - S^*, \varepsilon x_2 = E - E^*, \varepsilon x_3 = A - A^*, \varepsilon x_4 = V - V^*$ and $\varepsilon x_5 = Q - Q^*$. The equilibrium point of (2.1) is shifted to the origin, and the equation is expressed in vector form as follows:

$$\frac{dX(t)}{dt} = A_1 X(t) + A_2 X(t-\tau) + F,$$

$$A_1 = \begin{pmatrix} H_{11} & 0 & H_{13} & H_{14} & H_{15} \\ H_{21} & H_{22} & H_{23} & H_{24} & -H_{15} \\ 0 & H_{32} & H_{33} & 0 & 0 \\ 0 & 0 & H_{43} & H_{44} & 0 \\ 0 & H_{52} & 0 & 0 & H_{55} \end{pmatrix},$$

$$A_2 = \begin{pmatrix} 0 & 0 & 0 & 0 & -H_{15} \\ 0 & 0 & 0 & 0 & H_{15} \\ 0 & 0 & 0 & 0 & 0 \\ 0 & 0 & 0 & 0 & 0 \\ 0 & 0 & 0 & 0 & 0 \end{pmatrix},$$

in which

$$\begin{gathered} H_{11} = -\mu - \tfrac{\beta_0 A^*}{N}; H_{13} = -\tfrac{\beta_0 S^*}{N}; H_{14} = \Gamma; H_{15} = \tfrac{\beta_0 k A^* S^*}{N}; \\ H_{21} = \tfrac{\beta_0 A^*}{N}; H_{22} = -\varphi - \mu; H_{23} = \tfrac{\beta_g V^*}{N} + \tfrac{\beta_0 S^*}{N}; H_{24} = \tfrac{\beta_g A^*}{N}; \\ H_{32} = \alpha\varphi; H_{33} = -\rho - \mu - \delta; H_{43} = -\tfrac{\beta_g V^*}{N}; H_{44} = -\tfrac{\beta_g A^*}{N} - \Gamma - \mu; \\ H_{52} = -(\alpha - 1)\varphi; H_{55} = -\gamma - \mu - \delta. \end{gathered}$$

Without Gaussian white noise, (2.1) can be linearized as follows.

$$\begin{aligned} \frac{dx_1}{dt} &= -\left(\frac{\beta_0 A^*}{N} + \mu\right) x_1 - \frac{\beta_0 S^*}{N} x_3 + \Gamma x_4 + A^* S^* \frac{\beta_0 k}{N} \left(x_5 - x_5\left(t - \tau\right)\right), \\ \frac{dx_2}{dt} &= \frac{\beta_0 A^*}{N} x_1 - \left(\mu + \varphi\right) x_2 + \left(\frac{\beta_0 S^*}{N} + \frac{\beta_g V^*}{N}\right) x_3 + \frac{\beta_g A^*}{N} x_4 - A^* S^* \frac{\beta_0 k}{N} \left(x_5 - x_5\left(t - \tau\right)\right), \\ \frac{dx_3}{dt} &= \alpha\varphi x_2 - \left(\delta + \mu + \rho\right) x_3, \\ \frac{dx_4}{dt} &= -\frac{\beta_g V^*}{N} x_3 - \left(\Gamma + \mu + \frac{\beta_g A^*}{N}\right) x_4, \\ \frac{dx_5}{dt} &= (1 - \alpha)\varphi x_2 - \left(\gamma + \delta + \mu\right) x_5. \end{aligned} \tag{2.3}$$

The characteristic equation corresponding to (2.3) is

$$\left|\lambda I - A_1 - A_2 e^{-\lambda\tau}\right| = \left(\lambda + \Gamma + \mu + \frac{\beta_g A^*}{N}\right)\left(\lambda + \delta + \mu + \rho\right)\left(f_1\left(\lambda\right) - f_2\left(\lambda\right)\right) = 0, \tag{2.4}$$

where $f_1\left(\lambda\right) = \left(\lambda + \frac{\beta_g A^*}{N} + \mu\right)\left(\lambda + \mu + \varphi\right)\left(\lambda + \gamma + \delta + \mu\right)$, $f_2\left(\lambda\right) = \left(1 - \alpha\right)\varphi A^* S^* \frac{\beta_0 k}{N}\left(1 - e^{-\lambda\tau}\right)\left(\lambda + \mu\right)$.

Given that $\lambda_1 = -\left(\Gamma + \mu + \frac{\beta_g A^*}{N}\right)$, $\lambda_2 = -\left(\delta + \mu + \rho\right)$ and $f_2\left(0\right) = 0$, whether or not 0 is the root of the characteristic equation relies on whether $f_1(0) = 0$. Since $f_1(0) > 0$, it follows that 0 cannot be the root of the characteristic equation given by (2.4).

In order to determine if endemic diseases are stable at their equilibrium point when $\tau = 0$, the characteristic equation given by (2.4) is then transformed into the following.

$$\left(\lambda + \Gamma + \mu + \tfrac{\beta_g A^*}{N}\right)\left(\lambda + \delta + \mu + \rho\right) f_1\left(\lambda\right) = 0.$$

Hence, $\lambda_3 = -\left(\frac{\beta_g A^*}{N} + \mu\right)$, $\lambda_4 = -\left(\mu + \varphi\right)$ and $\lambda_5 = -\left(\gamma + \delta + \mu\right)$. All roots of the characteristic equation (2.4) have negative real parts, and the equilibrium point of endemic diseases is locally asymptotically stable.

Following this, take into account the scenario in which $\tau > 0$, $\lambda = i\omega$ and the characteristic equation are equivalent to

$$f_1\left(i\omega\right) - f_2\left(i\omega\right) = 0. \tag{2.5}$$

Separating the real part from the imaginary part, we get

$$\begin{aligned}
\sin\omega\tau &= \frac{\omega\left(\gamma+\delta+\varphi+2\mu+\frac{\beta_g A^*}{N}\right)}{(1-\alpha)\varphi A^* S^*\frac{\beta_0 k}{N}} - \frac{\omega\frac{\beta_g A^*}{N}\varphi(\gamma+\delta)}{(1-\alpha)\varphi A^* S^*\frac{\beta_0 k}{N}(\omega^2+\mu^2)},\\
\cos\omega\tau &= \frac{\omega^2-(\gamma+\delta+\mu+\varphi)\left(\mu+\frac{\beta_g A^*}{N}\right)-\varphi(\gamma+\delta)}{(1-\alpha)\varphi A^* S^*\frac{\beta_0 k}{N}} - \frac{\mu\varphi(\gamma+\delta)\frac{\beta_g A^*}{N}}{(\omega^2+\mu^2)(1-\alpha)\varphi A^* S^*\frac{\beta_0 k}{N}} + 1.
\end{aligned} \tag{2.6}$$

Squaring and adding together the two equations in (2.6), we have

$$\omega^8 + d_1\omega^6 + d_2\omega^4 + d_3\omega^2 + d_4 = 0. \tag{2.7}$$

Writing $z = \omega^2$, (2.7) is equivalent to

$$L(z) = z^4 + d_1 z^3 + d_2 z^2 + d_3 z + d_4 = 0, \tag{2.8}$$

where

$$\begin{aligned}
d_1 &= (\gamma+\delta+\varphi+2\mu)^2 + 2(1-\alpha)\varphi A^* S^*\frac{\beta_0 k}{N} > 0,\\
d_2 &= 2\left(\gamma+\delta+\varphi+2\mu+\frac{\beta_g A^*}{N}\right)\left(\mu^2\left(\gamma+\delta+\varphi+2\mu+\frac{\beta_g A^*}{N}\right)-\frac{\beta_g A^*}{N}\varphi(\gamma+\delta)\right)\\
&\quad + \left(\mu^2-H\right)^2 + 2(1-\alpha)\varphi A^* S^*\frac{\beta_0 k}{N}\left(2\mu^2-H\right) - \left(2\mu^2 H + 2\mu\varphi(\gamma+\delta)\frac{\beta_g A^*}{N}\right),\\
d_3 &= \left(\mu^2\left(\gamma+\delta+\varphi+2\mu+\frac{\beta_g A^*}{N}\right)-\frac{\beta_g A^*}{N}\varphi(\gamma+\delta)\right)^2\\
&\quad + 2\left(\mu^2-H\right)\left((1-\alpha)\varphi A^* S^*\frac{\beta_0 k}{N}\mu^2 - \left(\mu^2 H + \mu\varphi(\gamma+\delta)\frac{\beta_g A^*}{N}\right)\right)\\
&\quad - (1-\alpha)\varphi A^* S^*\frac{\beta_0 k}{N}\left(2\mu^2 H + 2\mu\varphi(\gamma+\delta)\frac{\beta_g A^*}{N}\right),\\
d_4 &= \left(\mu^2 H + \mu\varphi(\gamma+\delta)\frac{\beta_g A^*}{N}\right)^2 - \mu^2(1-\alpha)\varphi A^* S^*\frac{\beta_0 k}{N}\left(2\mu^2 H + 2\mu\varphi(\gamma+\delta)\frac{\beta_g A^*}{N}\right),\\
H &= (\gamma+\delta+\varphi+\mu)\left(\mu+\frac{\beta_g A^*}{N}\right) + \varphi(\gamma+\delta).
\end{aligned}$$

Since $\lim_{z\to\infty} L(z) = \infty$, if condition (H1): $\exists z^* > 0, L(z^*) < 0$ holds, (2.8) has at least one positive real root $z_i\,(1 \leqslant i \leqslant 4)$; thus, (2.7) has at least one positive real root $\omega_i = \sqrt{z_i}$. Equation (2.6) can be transformed as follows:

(1) If $\cos\omega_i\tau < 0$,

$$\tau_{ij} = \frac{1}{\omega_i}\arcsin\left[\frac{\omega_i\left(\gamma+\delta+\varphi+2\mu+\frac{\beta_g A^*}{N}\right)}{(1-\alpha)\varphi A^* S^*\frac{\beta_0 k}{N}} - \frac{\omega_i\frac{\beta_g A^*}{N}\varphi(\gamma+\delta)}{(1-\alpha)\varphi A^* S^*\frac{\beta_0 k}{N}\left({\omega_i}^2+\mu^2\right)}\right] + \frac{(2j+1)\pi}{\omega_i}\,(j=0,1,2,\ldots); \tag{2.9}$$

(2) If $\cos\omega_i\tau > 0$ and $\sin\omega_i\tau > 0$,

$$\tau_{ij} = -\frac{1}{\omega_i}\arcsin\left[\frac{\omega_i\left(\gamma+\delta+\varphi+2\mu+\frac{\beta_g A^*}{N}\right)}{(1-\alpha)\varphi A^* S^*\frac{\beta_0 k}{N}} - \frac{\omega_i\frac{\beta_g A^*}{N}\varphi(\gamma+\delta)}{(1-\alpha)\varphi A^* S^*\frac{\beta_0 k}{N}\left(\omega_i{}^2+\mu^2\right)}\right] + \frac{2j\pi}{\omega_i}\,(j=0,1,2,...)\,; \tag{2.10}$$

(3) If $\cos\omega_i\tau > 0$ and $\sin\omega_i\tau < 0$,

$$\tau_{ij} = -\frac{1}{\omega_i}\arcsin\left[\frac{\omega_i\left(\gamma+\delta+\varphi+2\mu+\frac{\beta_g A^*}{N}\right)}{(1-\alpha)\varphi A^* S^*\frac{\beta_0 k}{N}} - \frac{\omega_i\frac{\beta_g A^*}{N}\varphi(\gamma+\delta)}{(1-\alpha)\varphi A^* S^*\frac{\beta_0 k}{N}\left(\omega_i{}^2+\mu^2\right)}\right] + \frac{(2j+2)\pi}{\omega_i}\,(j=0,1,2,...)\,. \tag{2.11}$$

Defining $\tau_0 = \min\{\tau_{i0}, i = 1,2,3,4,5\}$, when $\tau = \tau_0$, $\lambda = \pm i\omega_0\,(\omega_0 > 0)$ denotes a pair of pure imaginary roots of (2.4).

Theorem 2.2. If $R_0 > 1$ and H1 and H2: $m = \left(-3\omega_0{}^2+b\right)\left(-c\omega_0{}^2\cos\omega_0\tau_0 + d\omega_0\sin\omega_0\tau_0\right) + 2a\omega_0\left(d\omega_0\cos\omega_0\tau_0 + c\omega_0{}^2\sin\omega_0\tau_0\right) - c^2\omega_0{}^2 \neq 0$ are satisfied, the system will generate Hopf bifurcation at the endemic equilibrium point.

Proof. Differentiating the two sides of (2.5) with respect to τ, the Hopf transversality condition is as follows:

$$\left(\frac{d\lambda}{d\tau}\right)^{-1} = \frac{3\lambda^2+2a\lambda+b}{(c\lambda^2+d\lambda)\,e^{-\lambda\tau}} + \frac{1}{\lambda^2+\mu\lambda} - \frac{\tau}{\lambda},$$

where $a = \frac{\beta_g A^*}{N} + 3\mu + \varphi + \gamma + \delta$,
$b = \left(\frac{\beta_g A^*}{N}+\mu\right)(\mu+\varphi) + \left(\frac{\beta_g A^*}{N}+\mu\right)(\gamma+\delta+\mu) + (\mu+\varphi)(\gamma+\delta+\mu)$,
$c = -(1-\alpha)\varphi A^* S^*\frac{\beta_0 k}{N}$,
$d = \mu c$.

$$\mathrm{Re}\left(\frac{d\lambda}{d\tau}\right)^{-1}\Bigg|_{\tau=\tau_0} = \frac{\left(-3\omega_0{}^2+b\right)\left(-c\omega_0{}^2\cos\omega_0\tau_0 + d\omega_0\sin\omega_0\tau_0\right) + 2a\omega_0\left(d\omega_0\cos\omega_0\tau_0 + c\omega_0{}^2\sin\omega_0\tau_0\right) - c^2\omega_0{}^2}{c^2\left(\omega_0{}^4+\mu^2\omega_0{}^2\right)}.$$

$\mathrm{Re}\left(\frac{d\lambda}{d\tau}\right)$ and $\mathrm{Re}\left(\frac{d\lambda}{d\tau}\right)^{-1}$ have the same signs. Therefore, if condition (H2) holds, according to Hopf bifurcation theory, Hopf bifurcation occurs at $\tau = \tau_0$, and the theorem is proved. □

3. Reduction and stochastic bifurcation of systems

In this section, the stochastic center manifold theorem is used to convert the stochastic differential equation with time delay into a stochastic differential equation.

Assuming that $\left(i\omega - A_1 - A_2 e^{-i\omega\tau_0}\right)q(0) = 0$, $q(0)$ is the eigenvector. Let $q(\theta) = q(0)e^{i\omega\theta}$, and, combined with Euler's formula, we have that $\Phi(\theta) = \begin{pmatrix}\phi_1(\theta) & \phi_2(\theta)\end{pmatrix}$, where $\phi_1(\theta) = \mathrm{Re}\,(q(\theta))$ and $\phi_2(\theta) = \mathrm{Im}\,(q(\theta))$. Then, we obtain

$$\Phi(\theta) = \begin{pmatrix}\phi_{11}(\theta) & \phi_{21}(\theta)\\ \phi_{12}(\theta) & \phi_{22}(\theta)\\ \phi_{13}(\theta) & \phi_{23}(\theta)\\ \phi_{14}(\theta) & \phi_{24}(\theta)\\ \phi_{15}(\theta) & \phi_{25}(\theta)\end{pmatrix}, -\tau \leqslant \theta \leqslant 0,$$

$$\phi_{11}(\theta) = \frac{N\cos\omega_0\theta}{\beta_0 A^*}\left(\mu+\varphi-\left(\frac{\beta_0 S^*}{N}+\frac{\beta_g V^*}{N}\right)\frac{\alpha\varphi(\delta+\mu+\rho)}{(\delta+\mu+\rho)^2+{\omega_0}^2}+\frac{{\beta_g}^2 A^* V^*\varphi\alpha}{N\left((\delta+\mu+\rho)^2+{\omega_0}^2\right)}\right)$$
$$+\frac{(\delta+\mu+\rho)\left(A^*\beta_g+\Gamma N+\mu N\right)-{\omega_0}^2 N}{\left(A^*\beta_g+\Gamma N+\mu N\right)^2+{\omega_0}^2N^2}\frac{N\cos\omega_0\theta}{\beta_0 A^*}$$
$$+S^*k\cos\omega_0\theta\left((\cos\omega_0\tau_0-1)\frac{(\alpha\varphi-\varphi)(\delta+\mu+\gamma)}{(\delta+\mu+\gamma)^2+{\omega_0}^2}-\sin\omega_0\tau_0\frac{(\alpha\varphi-\varphi)\omega_0}{(\delta+\mu+\gamma)^2+{\omega_0}^2}\right)$$
$$-\frac{N}{\beta_0 A^*}\sin\omega_0\theta\left(\omega_0+\left(\frac{\beta_0 S^*}{N}+\frac{\beta_g V^*}{N}\right)\frac{\alpha\varphi\omega_0}{(\delta+\mu+\rho)^2+{\omega_0}^2}\right)$$
$$-\frac{N}{\beta_0 A^*}\sin\omega_0\theta\left(-\frac{{\beta_g}^2 A^* V^*\varphi\alpha\left((\delta+\mu+\rho)\omega_0 N+\omega_0\left(A^*\beta_g+\Gamma N+\mu N\right)\right)}{N\left((\delta+\mu+\rho)^2+{\omega_0}^2\right)\left(\left(A^*\beta_g+\Gamma N+\mu N\right)^2+{\omega_0}^2N^2\right)}\right)$$
$$+S^*k\sin\omega_0\theta\left((\cos\omega_0\tau_0-1)\frac{(\alpha\varphi-\varphi)\omega_0}{(\delta+\mu+\gamma)^2+{\omega_0}^2}+\sin\omega_0\tau_0\frac{(\alpha\varphi-\varphi)(\delta+\mu+\gamma)}{(\delta+\mu+\gamma)^2+{\omega_0}^2}\right),$$

$$\phi_{21}(\theta) = \frac{N\sin\omega_0\theta}{\beta_0 A^*}\left(\mu+\varphi-\left(\frac{\beta_0 S^*}{N}+\frac{\beta_g V^*}{N}\right)\frac{\alpha\varphi(\delta+\mu+\rho)}{(\delta+\mu+\rho)^2+{\omega_0}^2}+\frac{{\beta_g}^2 A^* V^*\varphi\alpha}{N\left((\delta+\mu+\rho)^2+{\omega_0}^2\right)}\right)$$
$$+\frac{N\sin\omega_0\theta}{\beta_0 A^*}\frac{(\delta+\mu+\rho)\left(A^*\beta_g+\Gamma N+\mu N\right)-{\omega_0}^2 N}{\left(A^*\beta_g+\Gamma N+\mu N\right)^2+{\omega_0}^2N^2}$$
$$+S^*k\left((\cos\omega_0\tau_0-1)\frac{(\alpha\varphi-\varphi)(\delta+\mu+\gamma)}{(\delta+\mu+\gamma)^2+{\omega_0}^2}-\sin\omega_0\tau_0\frac{(\alpha\varphi-\varphi)\omega_0}{(\delta+\mu+\gamma)^2+{\omega_0}^2}\right)\sin\omega_0\theta$$
$$+\frac{N\cos\omega_0\theta}{\beta_0 A^*}\omega_0+\left(\frac{\beta_0 S^*}{N}+\frac{\beta_g V^*}{N}\right)\frac{\alpha\varphi\omega_0}{(\delta+\mu+\rho)^2+{\omega_0}^2}$$
$$-\frac{{\beta_g}^2 A^* V^*\varphi\alpha\left((\delta+\mu+\rho)\omega_0 N+\omega_0\left(A^*\beta_g+\Gamma N+\mu N\right)\right)}{N\left((\delta+\mu+\rho)^2+{\omega_0}^2\right)\left(\left(A^*\beta_g+\Gamma N+\mu N\right)^2+{\omega_0}^2N^2\right)}\frac{N\cos\omega_0\theta}{\beta_0 A^*}$$
$$+S^*k\left(-(\cos\omega_0\tau_0-1)\frac{(\alpha\varphi-\varphi)\omega_0}{(\delta+\mu+\gamma)^2+{\omega_0}^2}-\frac{\sin\omega_0\tau_0(\alpha\varphi-\varphi)(\delta+\mu+\gamma)}{(\delta+\mu+\gamma)^2+{\omega_0}^2}\right)\cos\omega_0\theta,$$

$$\phi_{12}(\theta) = \cos\omega_0\theta,$$

$$\phi_{22}(\theta) = \sin\omega_0\theta,$$

$$\phi_{13}(\theta) = \frac{\alpha\varphi(\delta+\mu+\rho)}{(\delta+\mu+\rho)^2+{\omega_0}^2}\cos\omega_0\theta+\frac{\alpha\varphi\omega_0}{(\delta+\mu+\rho)^2+{\omega_0}^2}\sin\omega_0\theta,$$

$$\phi_{23}(\theta) = \frac{\alpha\varphi(\delta+\mu+\rho)}{(\delta+\mu+\rho)^2+{\omega_0}^2}\sin\omega_0\theta-\frac{\alpha\varphi\omega_0}{(\delta+\mu+\rho)^2+{\omega_0}^2}\cos\omega_0\theta,$$

$$\phi_{14}(\theta) = -\frac{\alpha\varphi\upsilon\beta_g\left[(\delta+\mu+\rho)\left(A^*\beta_g+\Gamma N+\mu N\right)-{\omega_0}^2 N\right]}{\left[(\delta+\mu+\rho)^2+\omega_0^2\right]\left[\left(A^*\beta_g+\Gamma N+\mu N\right)^2+\omega_0^2 N^2\right]}\cos\omega_0\theta$$
$$-\frac{\alpha\varphi\upsilon\beta_g\left[\omega_0 N(\delta+\mu+\rho)+\left(A^*\beta_g+\Gamma N+\mu N\right)\omega_0\right]}{\left(\delta+\mu+\rho+a\beta_g+\Gamma N+\mu N-{\omega_0}^2 N\right)^2+\omega_0^2\left(A^*\beta_g+\Gamma N+\mu N+\delta+\mu+\rho\right)^2}\sin\omega_0\theta,$$

$$\phi_{24}(\theta) = -\frac{\alpha\varphi\upsilon\beta_g\left[(\delta+\mu+\rho)\left(A^*\beta_g+\Gamma N+\mu N\right)-{\omega_0}^2 N\right]}{\left[(\delta+\mu+\rho)^2+\omega_0^2\right]\left[\left(A^*\beta_g+\Gamma N+\mu N\right)^2+\omega_0^2 N^2\right]}\sin\omega_0\theta$$
$$+\frac{\alpha\varphi\upsilon\beta_g\left[\omega_0 N(\delta+\mu+\rho)+\left(A^*\beta_g+\Gamma N+\mu N\right)\omega_0\right]}{\left(\delta+\mu+\rho+a\beta_g+\Gamma N+\mu N-{\omega_0}^2 N\right)^2+\omega_0^2\left(A^*\beta_g+\Gamma N+\mu N+\delta+\mu+\rho\right)^2}\cos\omega_0\theta,$$

$$\phi_{15}(\theta) = -\frac{(\alpha\varphi-\varphi)(\delta+\mu+\gamma)}{(\delta+\mu+\gamma)^2+{\omega_0}^2}\cos\omega_0\theta-\frac{\omega_0(\alpha\varphi-\varphi)}{(\delta+\mu+\gamma)^2+{\omega_0}^2}\sin\omega_0\theta,$$

$$\phi_{25}(\theta) = -\frac{(\alpha\varphi-\varphi)(\delta+\mu+\gamma)}{(\delta+\mu+\gamma)^2+{\omega_0}^2}\sin\omega_0\theta+\frac{\omega_0(\alpha\varphi-\varphi)}{(\delta+\mu+\gamma)^2+{\omega_0}^2}\cos\omega_0\theta,$$

According to the adjoint relation of $\Phi(\theta)$ and $\Psi(s)$, we get

$$\Psi(s) = \begin{pmatrix}\psi_1(s)\\ \psi_2(s)\end{pmatrix} = \begin{pmatrix}l\psi_{11}(s) & \psi_{12}(s) & \psi_{13}(s) & \psi_{14}(s) & \psi_{15}(s)\\ \psi_{21}(s) & \psi_{22}(s) & \psi_{23}(s) & \psi_{24}(s) & \psi_{25}(s)\end{pmatrix},$$

$$\psi_{11}(s) = \cos\omega_0 s,$$
$$\psi_{21}(s) = \sin\omega_0 s,$$
$$\psi_{12}(s) = \left(\frac{\mu N}{A^*\beta_0}+1\right)\cos\omega_0 s+\frac{N\omega_0}{A^*\beta_0}\sin\omega_0 s,$$
$$\psi_{22}(s) = \left(\frac{\mu N}{A^*\beta_0}+1\right)\sin\omega_0 s-\frac{N\omega_0}{A^*\beta_0}\cos\omega_0 s,$$
$$\psi_{13}(s) = \left\{\frac{(\alpha-1)}{\alpha}\frac{kS^*\left[(\gamma+\delta+\mu)(\mu-\mu\cos\omega_0\tau_0-\omega_0\sin\omega_0\tau_0)-\omega_0(-\omega_0-\mu\sin\omega_0\tau_0+\omega_0\cos\omega_0\tau_0)\right]}{(\gamma+\delta+\mu)^2+\omega^2}\right.$$
$$\left.+\frac{1}{\alpha\varphi}\left[\frac{\mu N+A^*\beta_0}{A^*\beta_0}(\mu+\varphi)-\frac{N{\omega_0}^2}{A^*\beta_0}\right]\right\}\cos\omega_0 s+\left\{\frac{N\omega_0(\mu+\varphi)}{A^*\beta_0}+\frac{\omega_0(\mu N+A^*\beta_0)}{A^*\beta_0}-\frac{(\alpha-1)}{\alpha}\right.$$
$$\left.\frac{kS^*\left[(\gamma+\delta+\mu)(-\omega_0-\mu\sin\omega_0\tau_0+\omega_0\cos\omega_0\tau_0)+\omega_0(\mu-\mu\cos\omega_0\tau_0-\omega_0\sin\omega_0\tau_0)\right]}{(\gamma+\delta+\mu)^2+\omega^2}\right\}\sin\omega_0 s,$$

$$\psi_{23}(s) = \left\{\frac{(\alpha-1)}{\alpha}\frac{kS^*\left[(\gamma+\delta+\mu)(\mu-\mu\cos\omega_0\tau_0-\omega_0\sin\omega_0\tau_0)-\omega_0(-\omega_0-\mu_0\sin\omega_0\tau_0+\omega_0\cos\omega_0\tau_0)\right]}{(\gamma+\delta+\mu)^2+\omega^2}\right.$$
$$\left.+\frac{1}{\alpha\varphi}\left[\frac{\mu N+A^*\beta_0}{A^*\beta_0}(\mu+\varphi)-\frac{N{\omega_0}^2}{A^*\beta_0}\right]\right\}\sin\omega_0 s+\left\{-\frac{N\omega_0(\mu+\varphi)}{A^*\beta_0}-\frac{\omega_0(\mu N+A^*\beta_0)}{A^*\beta_0}\right.$$
$$\left.+\frac{(\alpha-1)}{\alpha}\frac{kS^*\left[(\gamma+\delta+\mu)(-\omega_0-\mu_0\sin\omega_0\tau_0+\omega_0\cos\omega_0\tau_0)+\omega_0(\mu-\mu\cos\omega_0\tau_0-\omega_0\sin\omega_0\tau_0)\right]}{(\gamma+\delta+\mu)^2+\omega^2}\right\}\cos\omega_0 s,$$

$$\psi_{14}(s) = -\frac{(-\Gamma N\beta_0 - \mu N\beta_g - A^*\beta_0\beta_g)\left(\Gamma N + \mu N + A^*\beta_g\right) - N^2\omega^2\beta_g}{\beta_0\left[(\Gamma N + \mu N + A^*\beta_g)^2 + N^2\omega^2\right]}\cos\omega_0 s$$
$$+ \frac{\left(\Gamma N + \mu N + A^*\beta_g\right)N\omega\beta_g}{\beta_0\left[(\Gamma N + \mu N + A^*\beta_g)^2 + N^2\omega^2\right]}\sin\omega_0 s,$$

$$\psi_{24}(s) = -\frac{(-\Gamma N\beta_0 - \mu N\beta_g - A^*\beta_0\beta_g)\left(\Gamma N + \mu N + A^*\beta_g\right) - N^2\omega^2\beta_g}{\beta_0\left[(\Gamma N + \mu N + A^*\beta_g)^2 + N^2\omega^2\right]}\sin\omega_0 s$$
$$- \frac{\left(\Gamma N + \mu N + A^*\beta_g\right)N\omega\beta_g}{\beta_0\left[(\Gamma N + \mu N + A^*\beta_g)^2 + N^2\omega^2\right]}\cos\omega_0 s,$$
$$\psi_{15}(s) = \frac{kS^*\left[(\gamma+\delta+\mu)(\mu - \mu\cos\omega_0\tau_0 - \omega_0\sin\omega_0\tau_0) + \omega_0(\omega_0 + \mu_0\sin\omega_0\tau_0 - \omega_0\cos\omega_0\tau_0)\right]}{(\gamma+\delta+\mu)^2 + \omega^2}\cos\omega_0 s$$
$$- \frac{kS^*\left[(\gamma+\delta+\mu)(-\omega_0 - \mu\sin\omega_0\tau_0 + \omega_0\cos\omega_0\tau_0) + \omega_0(\mu - \mu\cos\omega_0\tau_0 - \omega_0\sin\omega_0\tau_0)\right]}{(\gamma+\delta+\mu)^2 + \omega^2}\sin\omega_0 s,$$
$$\psi_{25}(s) = \frac{kS^*\left[(\gamma+\delta+\mu)(\mu - \mu\cos\omega_0\tau_0 - \omega_0\sin\omega_0\tau_0) - \omega_0(-\omega_0 - \mu_0\sin\omega_0\tau_0 + \omega_0\cos\omega_0\tau_0)\right]}{(\gamma+\delta+\mu)^2 + \omega^2}\sin\omega_0 s$$
$$+ \frac{kS^*\left[(\gamma+\delta+\mu)(-\omega_0 - \mu_0\sin\omega_0\tau_0 + \omega_0\cos\omega_0\tau_0) + \omega_0 ks(\mu - \mu\cos\omega_0\tau_0 - \omega_0\sin\omega_0\tau_0)\right]}{(\gamma+\delta+\mu)^2 + \omega^2}\cos\omega_0 s.$$

The solution space C of the linearized equation is spanned by the two-dimensional subspace P, which is composed of pure, virtual eigenvalues at Hopf bifurcation points, and the infinite-dimensional subspace Q, which is composed of the other eigenvalues, that is, $C = P \oplus Q$. Furthermore, the basis for P is $\Phi(\theta)$ and $\Psi(s)$. We find that $\psi_j \in C\left([0,\tau], R^2\right)$ and $\phi_k \in C\left([-\tau, 0], R^2\right)$, $j,k = 1,2$. The center manifold $M_f \subseteq C([-\tau, 0], R^n)$ tangent to P is obtained. The defined bilinear operator is as follows:

$$\left(\psi_j(s), \varphi_k(\theta)\right) = \left(\psi_j(0), \varphi_k(0)\right) - \int_{-\tau}^{0}\int_{0}^{\tau}\psi_j(\zeta+\tau)[d\eta(\theta,\mu)]\varphi_k(\zeta)d\zeta,$$

where $\eta(\theta,\mu) = A_1\delta(\theta) - A_2\delta(\theta + \tau_0 + \mu)$ and $\delta(\theta)$ is the Dirac delta function.

Next, substituting $(\Psi(s), \Phi(\theta))$ into the bilinear function, the non-singular matrix is obtained:

$$(\Psi, \Phi)_{nsg} = \begin{pmatrix} n_{11} & n_{12} \\ n_{21} & n_{22} \end{pmatrix},$$

$$n_{11} = \phi_{11}(0)\psi_{11}(0) + \phi_{12}(0)\psi_{12}(0) + \phi_{13}(0)\psi_{13}(0) + \phi_{14}(0)\psi_{14}(0) + \phi_{15}(0)\psi_{15}(0)$$
$$- A^*S^*\frac{\beta_0 k}{2N}\left(\phi_{15}(0)\left(\frac{1}{\omega_0}\sin\omega_0\tau_0 + \tau_0\cos\omega_0\tau_0\right) + \phi_{25}(0)\tau_0\sin\omega_0\tau_0\right)$$
$$+ A^*S^*\frac{\beta_0 k}{N}\left(\frac{\psi_{12}(0)\phi_{15}(0) + \omega_0\tau_0\psi_{12}(0)\phi_{25}(0) - \omega_0\tau_0\psi_{22}(0)\phi_{15}(0) - \psi_{22}(0)\phi_{25}(0)}{2\omega_0}\sin\omega_0\tau_0\right.$$
$$\left. + \left(\frac{\tau_0}{2}\psi_{12}(0)\phi_{15}(0) + \frac{\tau_0}{2}\psi_{22}(0)\phi_{25}(0)\right)\cos\omega_0\tau_0\right),$$

$$
\begin{aligned}
n_{12} &= \phi_{21}(0)\psi_{11}(0) + \phi_{22}(0)\psi_{12}(0) + \phi_{23}(0)\psi_{13}(0) + \phi_{24}(0)\psi_{14}(0) + \phi_{25}(0)\psi_{15}(0) \\
&\quad - A^*S^*\frac{\beta_0 k}{N}\left(-\frac{\tau_0}{2}\phi_{15}(0)\sin\omega\tau_0 + \phi_{25}(0)\left(\frac{1}{2\omega_0}\sin\omega_0\tau_0 + \frac{\tau_0}{2}\cos\omega_0\tau_0\right)\right) \\
&\quad + A^*S^*\frac{\beta_0 k}{N}\left(\left(\frac{\tau_0}{2}\phi_{25}(0)\psi_{12}(0) - \frac{\tau_0}{2}\phi_{15}(0)\psi_{22}(0)\right)\cos\omega_0\tau_0\right. \\
&\quad \left. + \left(-\frac{\tau_0}{2}\phi_{15}(0)\psi_{12}(0) + \frac{1}{2\omega_0}\phi_{25}(0)\psi_{12}(0) + \frac{1}{2\omega_0}\phi_{15}(0)\psi_{22}(0) - \frac{\tau_0}{2}\phi_{25}(0)\psi_{22}(0)\right)\sin\omega_0\tau_0\right), \\
n_{21} &= \phi_{11}(0)\psi_{21}(0) + \phi_{12}(0)\psi_{22}(0) + \phi_{13}(0)\psi_{23}(0) + \phi_{14}(0)\psi_{24}(0) + \phi_{15}(0)\psi_{25}(0) \\
&\quad - as\frac{\beta_0 k}{N}\left(\frac{\tau_0}{2}\phi_{15}(0)\sin\omega\tau_0 + \phi_{25}(0)\left(\frac{1}{2\omega_0}\sin\omega_0\tau_0 - \frac{\tau_0}{2}\cos\omega_0\tau_0\right)\right) \\
&\quad + as\frac{\beta_0 k}{N}\left(\left(-\frac{\tau_0}{2}\phi_{25}(0)\psi_{12}(0) + \frac{\tau_0}{2}\phi_{15}(0)\psi_{22}(0)\right)\cos\omega_0\tau_0\right. \\
&\quad \left. + \left(\frac{\tau_0}{2}\phi_{15}(0)\psi_{12}(0) + \frac{1}{2\omega_0}\phi_{25}(0)\psi_{12}(0) + \frac{1}{2\omega_0}\phi_{15}(0)\psi_{22}(0) - \frac{\tau_0}{2}\phi_{25}(0)\psi_{22}(0)\right)\sin\omega_0\tau_0\right), \\
n_{22} &= \phi_{21}(0)\psi_{21}(0) + \phi_{22}(0)\psi_{22}(0) + \phi_{23}(0)\psi_{23}(0) + \phi_{24}(0)\psi_{24}(0) + \phi_{25}(0)\psi_{25}(0) \\
&\quad - as\frac{\beta_0 k}{N}\left(\phi_{15}(0)\left(-\frac{1}{2\omega_0}\sin\omega_0\tau_0 + \frac{\tau_0}{2}\cos\omega_0\tau_0\right) + \phi_{25}(0)\frac{\tau_0}{2}\sin\omega_0\tau_0\right) \\
&\quad + as\frac{\beta_0 k}{N}\left(\left(\frac{\tau_0}{2}\psi_{12}(0)\phi_{15}(0) + \frac{\tau_0}{2}\psi_{22}(0)\phi_{25}(0)\right)\cos\omega_0\tau_0\right. \\
&\quad \left. + \frac{-\phi_{15}(0)\psi_{12}(0) + \omega_0\tau_0\phi_{25}(0)\psi_{12}(0) - \omega_0\tau_0\phi_{15}(0)\psi_{22}(0) + \phi_{25}(0)\psi_{22}(0)}{2\omega_0}\sin\omega_0\tau_0\right).
\end{aligned}
$$

The normalization process for $\Psi(s)$ to $\bar{\Psi}(s)$ is $\bar{\Psi}(s) =< \Psi(s), \Phi(\theta) >^{-1} \Psi(\mathrm{s})$, and the result is as follows:

$$
\bar{\Psi}(s) = \begin{pmatrix} \bar{\psi}_{11}(s) & \bar{\psi}_{12}(s) & \bar{\psi}_{13}(s) & \bar{\psi}_{14}(s) & \bar{\psi}_{15}(s) \\ \bar{\psi}_{21}(s) & \bar{\psi}_{22}(s) & \bar{\psi}_{23}(s) & \bar{\psi}_{24}(s) & \bar{\psi}_{25}(s) \end{pmatrix}.
$$

Substituting $\left(\bar{\Psi}(s), \Phi(\theta)\right)$ into the bilinear function, the identity matrix is obtained:

$$
\left(\bar{\Psi}, \Phi\right)_{id} = \begin{pmatrix} 1 & 0 \\ 0 & 1 \end{pmatrix}.
$$

$X_t(\phi(\theta), \tau, \varepsilon)$ is the only solution of the original nonlinear delay differential equation, where $\phi(\theta) \in C$. By dividing $X_t(\phi(\theta), \tau, \varepsilon)$ and $\phi(\theta)$ into $X_t(\phi(\theta), \tau, \varepsilon) = x_t^P(\phi(\theta), \tau, \varepsilon) + x_t^Q(\phi(\theta), \tau, \varepsilon)$ and $\phi(\theta) = \phi^P(\theta) + \phi^Q(\theta)$, respectively, $x_t^P(\phi(\theta), \tau, \varepsilon)$ and $\phi^P(\theta)$ become members of the space P. $x_t^Q(\phi(\theta), \tau, \varepsilon)$ and $\phi^Q(\theta)$ belong to the space Q.

With regard to the definition of $\dot{\Phi}(\theta) = \Phi(\theta)B$, it can be expressed as $\Phi(\theta) = \Phi(0)e^{B\theta}, -\tau \leqslant \theta \leqslant 0$ and $\bar{\Psi}(s) = e^{Bs}\bar{\Psi}(0), 0 \leqslant s \leqslant \tau$, where $B = \begin{pmatrix} 0 & \omega_0 \\ -\omega_0 & 0 \end{pmatrix}$ as $\left(\bar{\Psi}, \Phi\right)_{id} = I$. Therefore,

the solution of the equation can be obtained through the projection of $\phi^P(\theta) = \Phi(\theta)B \in C$ onto the center manifold M_f for the integral equation $X_t(\phi(\theta), \tau, \varepsilon)$. By changing variables through the formula $x_t^P(\theta) = \Phi(\theta)y(t) + x_t^Q(\theta)$, where $y(t) \in R^2$, the first order approximation in ε for $\theta = -\tau$ is obtained.

$$
\begin{aligned}
x_1(t) &= \phi_{11}(0)\, y_1 + \phi_{21}(0)\, y_2,\\
x_2(t) &= y_1,\\
x_3(t) &= \phi_{13}(0)\, y_1 + \phi_{23}(0)\, y_2,\\
x_4(t) &= \phi_{14}(0)\, y_1 + \phi_{24}(0)\, y_2,\\
x_5(t) &= \phi_{15}(0)\, y_1 + \phi_{25}(0)\, y_2,\\
x_5(t-\tau) &= (\phi_{15}(0)\cos\omega_0\tau + \phi_{25}(0)\sin\omega_0\tau)\, y_1 - (\phi_{15}(0)\sin\omega_0\tau - \phi_{25}(0)\cos\omega_0\tau)\, y_2,\\
x_5'(t-\tau) &= (\omega_0\phi_{15}(0)\sin\omega_0\tau - \omega_0\phi_{25}(0)\cos\omega_0\tau)\, y_1 + (\omega_0\phi_{15}(0)\cos\omega_0\tau + \omega_0\phi_{25}(0)\sin\omega_0\tau)\, y_2.
\end{aligned}
$$

The solution to (2.1) on the center manifold $M_f = \{\phi \in C \mid \phi = \Phi y + h(y), h \in S\} \in C$ is given below.

$$X_t(\theta) = \Phi(\theta)\, y(t) + h(\theta, y(t)), \tag{3.1}$$

where $-\tau_0 \leqslant \theta \leqslant 0$.

We use the extended equation of $z_t(\theta)$ to represent (2.1) and calculate the center manifold as follows:

$$\dot{x}_t(\theta) = \begin{cases} \frac{d[z_t(\theta)]}{d\theta}, -\tau_0 \leq \theta < 0, \\ L[z_t(\theta)] + F[z_t(\theta)], \theta = 0, \end{cases} \tag{3.2}$$

where $L[z_t(\theta)]$ and $F[z_t(\theta)]$ are the linear and nonlinear parts of (2.1), respectively. After combining (3.1) with (3.2), we get

$$\left[\Phi(\theta) + D_y h(\theta, y(t))\right]\dot{y}(t) = \begin{cases} \Phi(\theta)\, By(t) + \frac{\partial h}{\partial \theta}, -\tau_0 \leqslant \theta < 0 \\ \Phi(0)\, By(t) + F\left[\Phi(\theta)\, y(t) + h(\theta, y(t))\right] + L(h(\theta, y(t))), \theta = 0. \end{cases}$$

Considering $< \bar{\Psi}(s), h(\theta, y(t)) >= 0$, here are the calculated stochastic ordinary differential equations:

$$
\begin{aligned}
\dot{y}_1(t) &= \omega_0 y_2(t) + \bar{\psi}_{11}(0)\, F_1 + \bar{\psi}_{12}(0)\, F_2 + \bar{\psi}_{14}(0)\, F_4,\\
\dot{y}_2(t) &= -\omega_0 y_1(t) + \bar{\psi}_{21}(0)\, F_1 + \bar{\psi}_{22}(0)\, F_2 + \bar{\psi}_{24}(0)\, F_4,
\end{aligned}
$$

where

$$
\begin{aligned}
F_1 = {} & \varepsilon^{\frac{1}{2}}\xi(t)\frac{\beta_0 A^* S^*(x_5(t) - x_5(t-\tau_0))}{N} + \varepsilon\tilde{\tau}A^*S^*\frac{\beta_0 k}{N}x_5'(t-\tau_0) - \frac{\varepsilon\beta_0 x_1(t)\, x_3(t)}{N}\\
& + \frac{(A^* x_1(t)\, x_5(t) + S^* x_3(t)\, x_5(t))\,\varepsilon\beta_0 l_1}{N} - \frac{\varepsilon\beta_0 l_1 (S^* x_3(t)\, x_5(t-\tau_0) + A^* x_1(t)\, x_5(t-\tau_0))}{N}\\
& + \frac{\left(-x_5(t)^2 + 2x_5(t)\, x_5(t-\tau_0) - x_5(t-\tau_0)^2\right)\varepsilon A^* S^* \beta_0 l_2}{N} + \varepsilon^2\Big(\frac{\beta_0 l_1 x_1(t)\, x_3(t)\,(x_5(t) - x_5(t-\tau_0))}{N}\\
& - \frac{\beta_0 l_2 (A^* x_1(t) + S^* x_3(t))}{N}(x_5(t)^2 + x_5(t-\tau_0)^2 - 2x_5(t)\, x_5(t-\tau_0))\\
& - \frac{A^* S^*}{N}\Big(\frac{1}{3}\beta_0 l_1 - \beta_0 l_3\Big)(x_5(t)^3 + 3x_5(t)\, x_5(t-\tau_0)^2 - x_5(t-\tau_0)^3 - 3x_5(t-\tau_0)\, x_5(t)^2)\Big),
\end{aligned}
$$

$$F_2 = -F_1 + \frac{\beta_g \varepsilon x_3 x_4}{N}, F_4 = -\frac{\beta_g \varepsilon x_3 x_4}{N},$$
$$l_1 = k + \varepsilon^{\frac{1}{2}} \xi(t), l_2 = k^2 + 2k\varepsilon^{\frac{1}{2}} \xi(t).$$

Carry out the polar coordinate transformation by using the stochastic averaging method [29]:

$$\begin{cases} y_1 = R(t) \cos\theta, \\ y_2 = -R(t) \sin\theta, \\ \theta = \omega_0 t + \varphi(t), \end{cases}$$

where $R(t)$ and $\varphi(t)$ are the amplitude and phase of the solution, respectively. We can obtain the stochastic ODEs with $R(t)$ and $\varphi(t)$:

$$\begin{cases} \dot{R}(t) = (\bar{\psi}_{11}(0) F_1 + \bar{\psi}_{12}(0) F_2 + \bar{\psi}_{14}(0) F_4) \cos\theta - (\bar{\psi}_{21}(0) F_1 + \bar{\psi}_{22}(0) F_2 + \bar{\psi}_{24}(0) F_4) \sin\theta, \\ \dot{\varphi}(t) = -\frac{1}{R} ((\bar{\psi}_{11}(0) F_1 + \bar{\psi}_{12}(0) F_2 + \bar{\psi}_{14}(0) F_4) \sin\theta + (\bar{\psi}_{21}(0) F_1 + \bar{\psi}_{22}(0) F_2 + \bar{\psi}_{24}(0) F_4) \cos\theta). \end{cases}$$

Since $R(t)$ and $\varphi(t)$ are both slow varying processes, the random averaging method is used to average time on the pseudo-period $\frac{2\pi}{\omega_0}$. The amplitude process after smoothing $R(t)$ is a Markov diffusion process, and the Itô equation is obtained as shown below.

$$\begin{aligned} dR &= m(R) dt + \sigma(R) dB(t), \\ m(R) &= \mu_1 R + \mu_2 R^3, \\ \sigma(R) &= \sqrt{\mu_3 R^2}, \\ \mu_1 &= \varepsilon \tilde{\tau} r_1 + K \varepsilon r_2, \\ \mu_2 &= \varepsilon^2 r_4, \\ \mu_3 &= K \varepsilon r_5. \end{aligned}$$

$R = 0$ is the equilibrium point of the system, whose Lyapunov exponent is

$$\begin{aligned} \lambda &= \lim_{t\to\infty} \frac{1}{t} \ln V = \lim_{t\to\infty} \frac{1}{t} \int_0^t \left\{ m'(R=0) - \frac{1}{2} \left[\sigma'(R=0)\right]^2 \right\} \mathrm{d}t \\ &= m'(R=0) - \frac{1}{2} \left[\sigma'(R=0)\right]^2 = \mu_1 - \frac{1}{2}\mu_3. \end{aligned}$$

When $\lambda < 0$, that is, $\mu_1 < \frac{1}{2}\mu_3$, the trivial solution to the equation is locally asymptotically stable. When $\lambda > 0$, that is, $\mu_1 > \frac{1}{2}\mu_3$, the trivial solution to the equation is unstable. Next, the global dynamic properties are obtained via boundary classification and the three-exponential method. When $\mu_2 < 0$, the right boundary $R \to +\infty$ is an entry boundary, and this condition is the premise of the following discussion. Because $m(0) = \sigma(0) = 0$, the left boundary belongs to the first kind of singular boundary. Its diffusion coefficient $\alpha = 2$, drift coefficient $\beta = 1$ and characteristic value $c = \frac{2\mu_1}{\mu_3}$. When $\frac{2\mu_1}{\mu_3} > 1$, the nontrivial stationary probability density exists in the system.

$$p(R) = \frac{C}{\sigma^2(R)} \exp\left[\int \frac{2m(R)}{\sigma^2(R)} \mathrm{d}R\right]$$

$$= \frac{C}{\mu_3} R^{\frac{2\mu_1}{\mu_3}-2} e^{\frac{\mu_2 R^2}{\mu_3}}.$$

Because $\alpha - \beta = 1$, the stationary probability density can be simplified as $p(R) = O(R^{c-\alpha})$. Dynamic bifurcation, also known as D-bifurcation, refers to a change in integrability. Phenomenological bifurcation, P-bifurcation, refers to a change of probability density image shape. Through analysis, D-bifurcation occurs at $\mu_1 = \frac{1}{2}\mu_3$, and P-bifurcation occurs at $\mu_1 = \mu_3$, as shown in Figure 2.

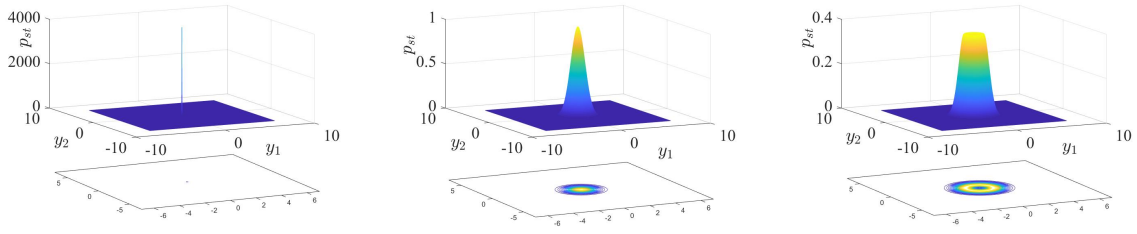

(a) $\mu_1 = -0.2, \mu_2 = -1, \mu_3 = 1$ (b) $\mu_1 = 0.999, \mu_2 = -1, \mu_3 = 1$ (c) $\mu_1 = 2, \mu_2 = -1, \mu_3 = 1$

Figure 2. P(D)-bifurcation diagram of the system.

4. Numerical simulation

In this section, in order to reveal the dynamic behavior of the system, we utilize a sample size of 100 and employ the Euler-Maruyama method to carry out the simulations. Based on the theoretical study in the preceding sections, time delay plays a vital role in studying the spread of infectious diseases as a bifurcation parameter. The stability of the system changes as the time delay rises, and the system has a periodic solution.

The basic reproductive number of the system in an undisturbed state $R_0 = 2.02741 > 1$ is determined using the numbers in Table 1, so the equilibrium point of endemic diseases exists in system (2.1) and is recorded as $P^*(S^*, E^*, A^*, V^*, Q^*, R^*)$, in which $S^* = 552030.54, E^* = 1405470.79, A^* = 87494.34, V^* = 4741153.57, Q^* = 71666.036, R^* = 3142180$. $L(0) = -10^{-12}$ and $m = 25.1664$, so both H1 and H2 are satisfied. Through the analysis in the second section, it is calculated that $\omega_0 = 0.302386$, $\tau_0 = 12.5623$ and Hopf bifurcation occurs at $\tau = \tau_0$.

Table 1. Parameter list.

Parameter	Value	Parameter	Value
μ	0.007	k	0.003
Γ	0.00015	Ω	75000
ρ	0.25	β_0	0.9
φ	0.02	β_g	0.81
α	0.8	N	10000000
ε	0.01	η	0.9
δ	0.000017	γ	1/14

The noise intensity was set to $K = 0$ and we drew the time series diagrams of S, E, A, V, Q, R with $\tau = 10$ and $\tau = 15$, as illustrated in Figures 3 and 4. When $\tau = 10 < \tau_0$, the endemic equilibrium point is stable, and when $\tau = 15 > \tau_0$, an infection periodically develops at the endemic equilibrium point. It should be mentioned that there is a time interval when the media reports the progress of infectious diseases. The system may oscillate if the delay of reporting the number of newly infected individuals with symptoms exceeds the threshold.

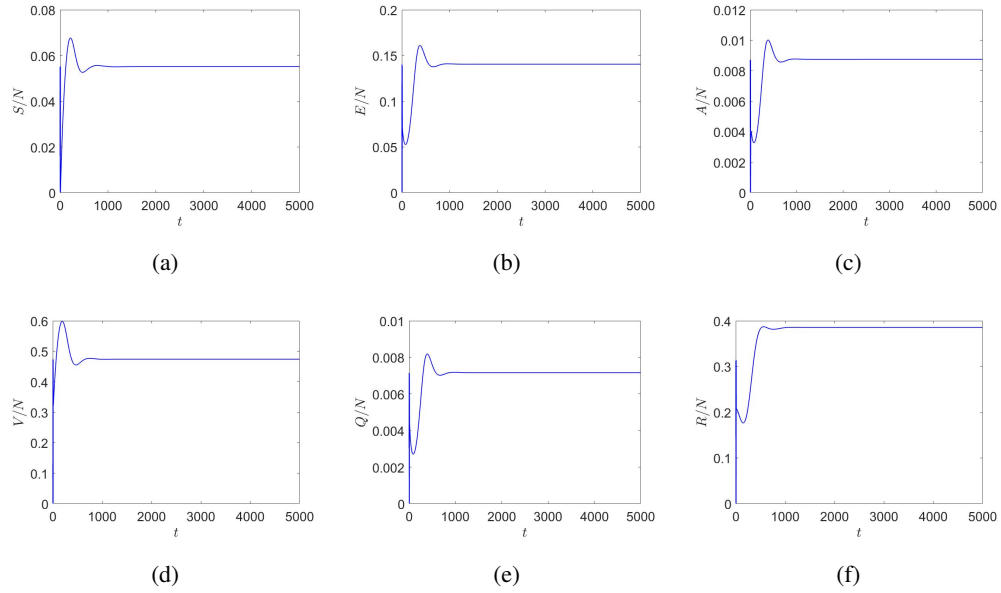

Figure 3. The time-series plots of S, E, A, V, Q, R for the parameter $\tau = 10 < \tau_0$.

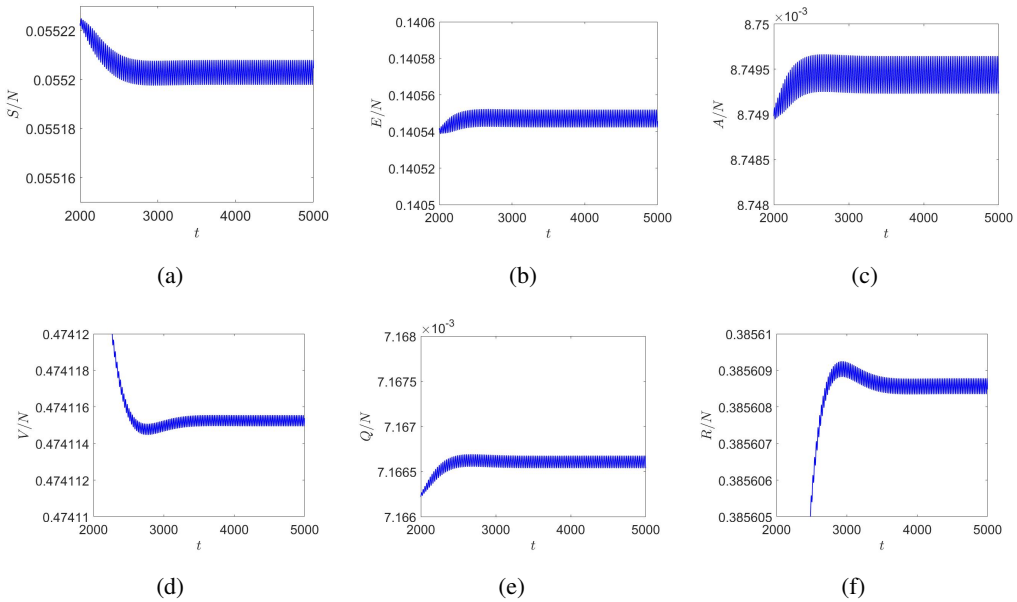

Figure 4. The time-series plots of S, E, A, V, Q, R for the parameter $\tau = 15 > \tau_0$.

Suppose that $k = 0.1$; then, $\tau_0 = 1.75$ can be determined; we applied $\tau = 10, 15, 20$ in system (2.1) correspondingly. Figure 5 depicts the oscillation of the Q/N time-series curve. Observing Figure 5, the number of symptomatic infections increases as the reporting time delay grows. By maintaining a reporting time delay below the threshold, it ensures that individuals can comprehend the epidemic situation and implement timely prevention and control measures. However, when the reporting time is delayed beyond the threshold, the public lacks access to relevant information, hampering their ability to make scientifically informed decisions and implement effective prevention measures. As a consequence, the number of infected individuals increases. As a result, the threshold τ_0 is extremely useful for the study, control and eradication of infectious illnesses.

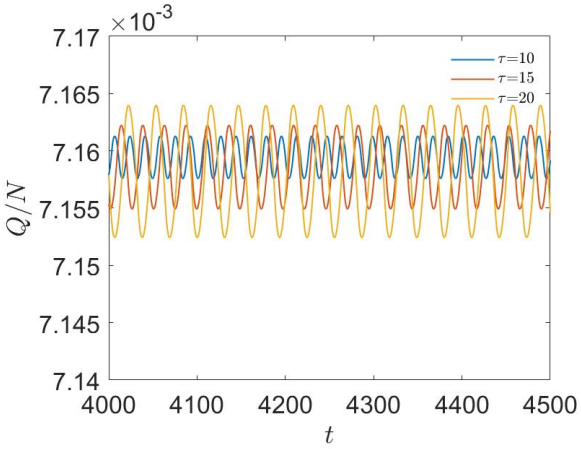

Figure 5. Effects of different time delays on periodic oscillation when $k = 0.1$.

We have chosen various sensitivity coefficients, k, and computed τ_0 accordingly. Based on these calculations, we have generated a line chart, as shown in Figure 6, illustrating the relationship between τ_0 and the sensitivity coefficient, k. It is discovered that τ_0 decreases as the sensitivity coefficient k increases. As the sensitivity coefficient increases, there is a corresponding rise in the level of attention people pay to the number of new symptomatic infections. Consequently, this increased sensitivity generates a higher demand for real-time reporting.

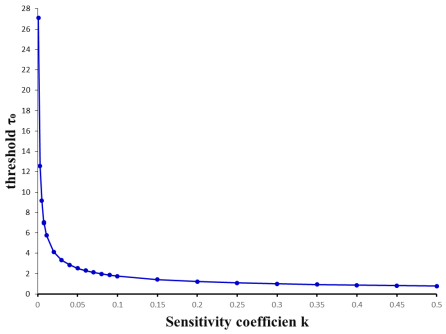

Figure 6. The curve of threshold changing with the sensitivity coefficient k.

The impact of the sensitivity coefficient k and reporting time delay on the progression of

infectious diseases is examined further below. Set $S(0) = 9999999$, $E(0) = 1$ and $A(0) = V(0) = Q(0) = R(0) = 0$ as the initial values, and set $K = 0.1$ and $k = 0.001$; then, we get $\tau_0 = 27.1083$. Set the reporting delays τ as 1, 8, 17 and 26 respectively. Figure 7(a) depicts a time-series plot showing the proportion of symptomatic infected patients in the crowd for various reporting delays. The increase of time delay τ only minimally influences the peak size, but it delays the arrival time of the peak. If $K = 0.1$ and $k = 0.4$, τ_0=0.85 is calculated, and then set τ equal to 0.1 and 0.85, respectively. Figure 7(b) depicts a time-series plot showing the proportion of symptomatic infected patients in the population. The increase in reporting delay diminishes the peak and delays its arrival. An appropriately prolonged reporting interval means that the number of reported new infections increases, which may causes public thinking and has a positive impact on epidemic prevention and control. Set $K = 0.1, \tau$=1 and k=0.2, 0.3, 0.4, 0.5 to create a time-series plot representing the fraction of symptomatic infected people in the population, as illustrated in Figure 8. The arrival time of the peak value is delayed as the sensitivity coefficient k increases, and the peak value decreases obviously. The increasing sensitivity coefficient k indicates that the public is more sensitive to the number of new symptomatic infections, which enhances public knowledge of protection and lowers the infection rate, resulting in a decrease in the number of infected people.

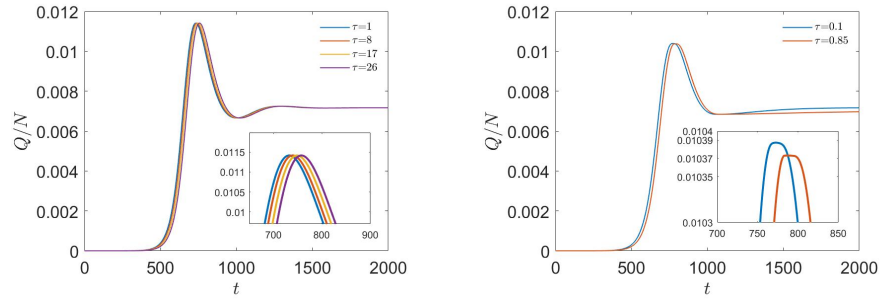

(a) k=0.001 (b) k=0.4

Figure 7. Time-series plots of Q/N for different reported delays τ.

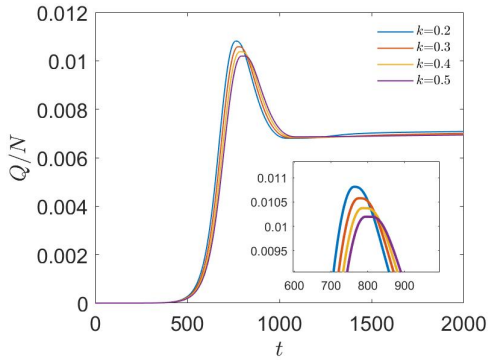

Figure 8. Time-series plots for Q/N given τ=1 and different sensitivity coefficients k.

Postponing the occurrence of the peak period can be advantageous for the government, as it enables the allocation of resources, thereby bolstering medical capabilities and providing additional time to realize the control of infectious diseases. By reducing the peak, the burden on medical resources can be mitigated and infected individuals can be brought to a manageable stage, ensuring adherence to medical standards during an outbreak. Hence, it is crucial for the media to exercise reasonable control over the timing of reporting and publicity efforts. When the sensitivity coefficient, denoted as k, remains constant, a reporting delay close to τ_0 can yield significant results with minimal effort. Additionally, it should be noted that the value of the sensitivity coefficient, k, can be subject to variation.

The random dynamic behavior close to τ_0 will now be then examined. Select noise intensity as the bifurcation parameter, set $\tau = 12.562 < \tau_0$, $\varepsilon = 0.00000001$ and refer to Table 1 for additional parameters. The third section's theoretical study reveals that the system will randomly bifurcate when $\mu_1 = \mu_3$, that is, when K=1.613. For Figure 9, we have selected a specific time period ranging from 3000d to 5000d to conduct simulations and generate the joint probability density diagram and marginal probability density diagram for susceptible persons (S) and symptomatic infected persons (Q) with noise intensity increasing from 1 to 200. The marginal probability map transforms from a single peak to a multi-peak structure as the noise intensity rises, and a random P-bifurcation takes place. A time-series plot of Q/N between $K = 1$ and $K = 200$ is shown in Figure 10(a) and 10(b). When the noise intensity is minimal, the system usually remains stable. When the noise intensity is high, the system oscillates, which implies that, as the noise intensity rises, so does the population of infected people. Let $\tau = 10$, $\varepsilon = 0.01$ and the noise intensity K traverse 1, 10, 15 and 20 in Figure 11. The variance of the random process considerably rises with the noise level over a period ranging from 4000d to 5000d. As can be seen from Figure 12(a) and 12(b), the noise intensity increases and the system loses stability over a period ranging from 2000d to 5000d. Social networking platforms like Twitter, Weibo and Facebook are often used, which has facilitated the spread of rumors that might potentially frighten the population [30, 31]. Furthermore, the dissemination of false information will impede the reporting of information and may encourage people to select inefficient preventative and control measures that cannot successfully control infectious diseases [32]. Therefore, media should convey the information to the public in a stable, objective and scientific manner.

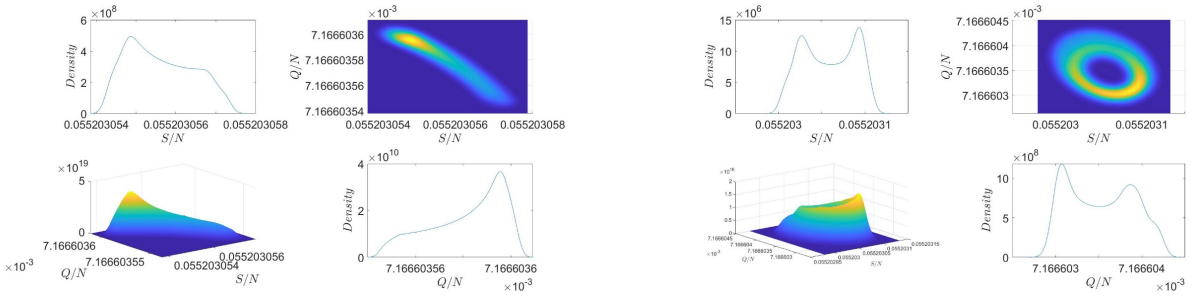

(a) $K = 1$ (b) $K = 200$

Figure 9. Probability density diagram with noise intensity K as the bifurcation parameter when $\tau = 12.562$.

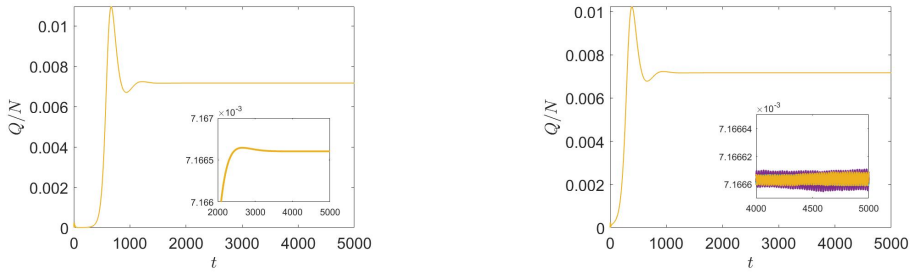

(a) K=1 (b) K=200

Figure 10. Time-series plots with noise intensity K as the bifurcation parameter when τ = 12.562. (a) K=1, (b) K=200.

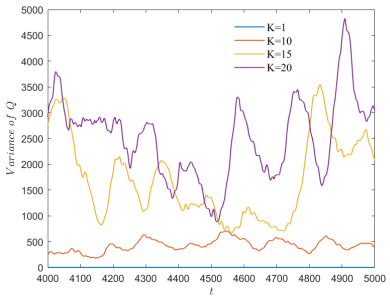

Figure 11. Variance plot of Q for different noise intensities at τ = 10, ε=0.01.

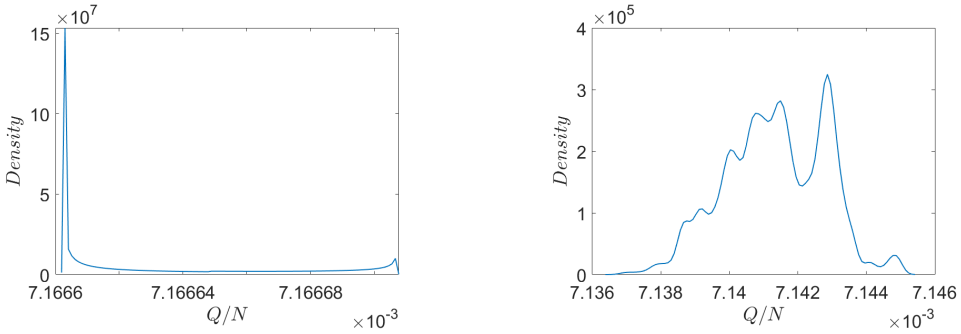

(a) K=0.0001 (b) K=20

Figure 12. The probability density diagram of Q/N with $\tau = 10, \varepsilon = 0.01$.

We normally believe that, when an epidemic strikes, the greater the media coverage, the better. However, as shown in Figure 6, τ_0 drops as the sensitivity coefficient increases, and the media's reporting time delay is restricted by human resources, technical equipment and so on. In some circumstances, the reporting delay will exceed the threshold τ_0. As the amplitude of the periodic oscillation increases, control methods must be changed over time, posing significant obstacles to epidemic prevention and control. Furthermore, before the health department can supply the information, vast volumes of noise information in the data must be collected and pre-processed. A

minor reporting time delay may reduce the accuracy of the reporting information and influence the system's stability. Governments should review whether publicity intensity matches correlative sectors' abilities to respond to emergencies and gather and analyze data. It will be self-defeating if the correlative sectors' capacity does not fulfill the threshold criteria. It is assumed that the correlative sectors' capacity can meet the τ_0 requirement, and we choose τ_0 as the reporting time.

With increased publicity intensity, the peak might occur considerably sooner, as indicated in Figure 13(a). In Figure 13(a), an increase in the value of k results in the peak arrival time being shifted forward by 20 days. Increasing the threshold by reducing the intensity of publicity can reduce work pressure in the health industry, but the peak size may increase, as illustrated in Figure 13(b). According to Figure 13(b), reducing the value of k leads to an increase in the peak number of symptomatic infections by 600 individuals.

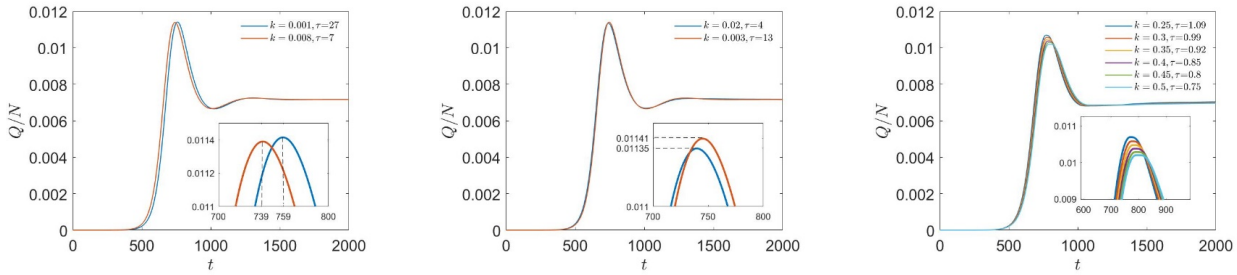

(a) (b) (c)

Figure 13. Time-series plots of different publicity strategies.

It should be emphasized that cultural factors influence the sensitivity coefficient k. It cannot be changed randomly with a change in publicity intensity, but it can change within an interval. In a group with a sense of duty, k is frequently greater. Figure 13(c) depicts a time-series plot mimicking k at various publicity intensities ranging from 0.25 to 0.5. We discovered that, assuming that the health department's capability can match the publicity intensity, the larger the publicity intensity, the smaller the peak, and the later the peak occurs. Of course, the sensitivity coefficient's growth has an upper bound. Following the previous research, we suspect that there is a k_0. When $k > k_0$, we should raise the degree of publicity. When $k < k_0$, the arrival time and peak value cannot be simultaneously optimized, and trade-offs must be made based on the actual scenario. The magnitude and timing of spikes have a substantial societal and economic impact, with overburdened healthcare systems increasing infectious mortality, direct morbidity and medical consequences [33]. As a result, the government should make appropriate publicity intensity based on current circumstances, such as medical resources, social stability and public welfare. The current sensitivity of society which can roughly reflect the change interval of the sensitivity coefficient under the action of media publicity, is also an important reference index for the government.

5. Conclusions

In this paper, a SEAVQR model with Gaussian white noise is established. Due to the process of data collection and preprocessing, there exists a temporal gap in reporting infectious diseases. We

discovered that an acceptable reporting time delay aids in the control of infectious illness spread. Hopf bifurcation occurs at $\tau = \tau_0$. Setting τ_0 as the reporting time-delay threshold, and under the condition that the reporting time delay is less than the threshold, the public can gain valuable insight into the epidemic situation and take prompt preventative and control actions. When the reporting time delay exceeds the threshold, a lack of public information on responses can lead to an increase in the number of infected people. If the reporting time delay exceeds the threshold, the larger the time delay, the greater the obstacle to the control of infectious diseases. The system takes into account the effect of noise on the transmission of infectious diseases. The dissemination of inaccurate information can hinder the public's ability to make informed judgments, and the proliferation of rumors can exacerbate the "fear effect," leading to an unstable system. When the reporting time delay approaches the threshold, the system may oscillate periodically if the noise intensity becomes larger. Therefore, the accuracy of reporting information and the timeliness of reporting should be considered by the government in the early control of the epidemic.

Furthermore, we discovered that increasing the reporting delay could postpone the arrival of the peak of symptomatic infected patients and minimize the peak of infection, giving us more precious time to control the epidemic. The same result can be obtained by increasing the sensitivity coefficient. In a stable state, adopting a longer reporting delay and the government enhancing public sensitivity through media awareness will help enhance medical treatment quality and living standards. As a result, while the sensitivity coefficient is fixed, it is better to set the reporting time delay around the threshold. However, we observe that increasing the sensitivity coefficient results in a drop in the stated delay threshold. The media's publicity intensity for the epidemic is not that the higher the intensity, the better. When the correlative departments' work abilities cannot meet the stronger publicity intensity, the public may be unable to adopt timely preventative and control measures due to low accuracy or big reporting delays, potentially leading to the spread of infectious illnesses becoming out of control. We also discovered the existence of k_0. When $k < k_0$, government increases in publicity intensity may cause the peak to arrive earlier. If the government decreases publicity intensity to raise the threshold at the expense of lowering the sensitivity coefficient, it will result in a peak increase and, to some extent, undermine public welfare. When $k > k_0$, however, the increase in publicity intensity could be helpful in postponing and lowering the peak.

To sum up, during the pandemic, the government should correctly understand the public's attitude toward this infectious disease. If the sensitivity k exceeds k_0, it should try its best to improve the sensitivity. If k is less than k_0, it is necessary to formulate appropriate publicity intensity for media publicity under the guidance of social and economic conditions and the ability of correlative departments in order to maximize benefits. In addition, the appropriate reporting time should be taken near the threshold. The media should grasp timeliness, accuracy and effectiveness in reporting. Code is available at https://github.com/Wangqiubao/HC_num_sim.

Use of AI tools declaration

The authors declare that they have not used artificial intelligence tools in the creation of this article.

Acknowledgments

This work was supported by the Natural Science Foundation of Hebei Province [A2021210011], the project of College Students' Innovation and Entrepreneurship Training Program 'Dynamics of stochastic delay model of COVID-19 diffusion' [202210107027], the Department of Education of Hebei Province [ZD2021335], Postgraduate Students Innovation Ability Training Fund Project of the Education Deparment of Hebei Province [CXZZSS2023083], the National Natural Science Foundation of China [Nos.11602151, 11872253, 12102274, 12072203],333 Talents Project of Hebei Province [No. A202005007] and the Hundred Excellent Innovative [No. SLRC2019037].

Conflict of interest

All authors declare no conflict of interest that could affect the publication of this paper

References

1. J. Bedford, J. Farrar, C. Ihekweazu, G. Kang, M. Koopmans, J. Nkengasong, A new twenty-first century science for effective epidemic response, *Nature*, **575** (2019), 130–136. https://doi.org/10.1038/s41586-019-1717-y
2. D. E. Bloom, D. Cadarette, Infectious disease threats in the 21st century: strengthening the global response, *Front. Immunol.*, **10** (2019). https://doi.org/10.3389/fimmu.2019.00549
3. W. O. Kermack, A. G. McKendrick, A contribution to the mathematical theory of epidemics, *Proc. Royal Soc. London. Series A*, **115** (1927), 700–721. https://doi.org/10.1098/rspa.1927.0118
4. I. Korolev, Identification and estimation of the SEIRD epidemic model for COVID-19, *J. Econometrics*, **220** (2021), 63–85. https://doi.org/10.1016/j.jeconom.2020.07.038
5. L. Basnarkov, SEAIR Epidemic spreading model of COVID-19, *Chaos Solitons Fract.*, **142** (2021), 110394. https://doi.org/10.1016/j.chaos.2020.110394
6. Z. Y. He, A. Abbes, H. Jahanshahi, N. D. Alotaibi, Y. Wang, Fractional-order discrete-time SIR epidemic model with vaccination: chaos and complexity, *Mathematics*, **10** (2022), 165. https://doi.org/10.3390/math10020165
7. X. Meng, Z. Cai, S. Si, D. Duan, Analysis of epidemic vaccination strategies on heterogeneous networks: based on SEIRV model and evolutionary game, *Appl. Math. Comput.*, **403** (2021), 126172. https://doi.org/10.1016/j.amc.2021.126172
8. K. Goel, A mathematical and numerical study of a SIR epidemic model with time delay, nonlinear incidence and treatment rates, *Theory Biosci.*, **138** (2019), 203–213. https://doi.org/10.1007/s12064-019-00275-5
9. Y. Liu, J. A. Cui, The impact of media coverage on the dynamics of infectious disease, *Int. J. Biomath.*, **1** (2008), 65–74. https://doi.org/10.1142/S1793524508000023
10. I. Z. Kiss, J. Cassell, M. Recker, P. L. Simon, The impact of information transmission on epidemic outbreaks, *Math Biosci.*, **225** (2010), 1–10. https://doi.org/10.1016/j.mbs.2009.11.009

11. Y. Xiao, S. Tang, J. Wu, Media impact switching surface during an infectious disease outbreak, *Sci. Rep.*, **5** (2015), 1–19. https://doi.org/10.1038/srep07838

12. D. Stellmach, I. Beshar, J. Bedford, P. Du Cros, Anthropology in public health emergencies: what is anthropology good for? *BMJ Global Health*, **3** (2018), e000534. http://dx.doi.org/10.1136/bmjgh-2017-000534

13. S. J. Heine, *Cultural Psychology*, New York: John Wiley and Sons, 2010. https://doi.org/10.1002/9780470561119.socpsy002037

14. J. Wu, R. Zuo, C. He, H. Xiong, K. Zhao, Z. Hu, The effect of information literacy heterogeneity on epidemic spreading in information and epidemic coupled multiplex networks, *Physica A: Statist. Mech. Appl.*, **596** (2022), 127119. https://doi.org/10.1016/j.physa.2022.127119

15. G. D.Webster, J. L. Howell, J. E. Losee, E. A. Mahar, V. Wongsomboon, Culture, COVID-19, and collectivism: A paradox of American exceptionalism? *Pers. Indiv. Differ.*, **178** (2021), 110853. https://doi.org/10.1016/j.paid.2021.110853

16. A. K. Misra, A. Sharma, J. B. Shukla, Modeling and analysis of effects of awareness programs by media on the spread of infectious diseases, *Math. Comput. Model.*, **53** (2011), 1221–1228. https://doi.org/10.1016/j.mcm.2010.12.005

17. E. Gutierrez, A. Rubli, T. Tavares, Information and behavioral responses during a pandemic: evidence from delays in COVID-19 death reports, *J. Dev. Econ.*, **154** (2022), 102774. https://doi.org/10.1016/j.jdeveco.2021.102774

18. Y. Cai, Y. Kang, M. Banerjee, W. Wang, A stochastic SIRS epidemic model with infectious force under intervention strategies, *J. Differ. Equ.*, **259** (2015), 7463–7502. https://doi.org/10.1016/j.jde.2015.08.024

19. Q. Liu, D. Jiang, T. Hayat, A. Alsaedi, Dynamical behavior of a stochastic epidemic model for cholera, *J. Franklin Inst.*, **356** (2019), 7486–7514. https://doi.org/10.1016/j.jfranklin.2018.11.056

20. B. Zhou, X. Zhang, D. Jiang, Dynamics and density function analysis of a stochastic SVI epidemic model with half saturated incidence rate, *Chaos Solitons Fract.*, **137** (2020), 109865. https://doi.org/10.1016/j.chaos.2020.109865

21. F. Li, S. Zhang, X. Meng, Dynamics analysis and numerical simulations of a delayed stochastic epidemic model subject to a general response function, *Comput. Appl. Math.*, **38** (2019), 1–30. https://doi.org/10.1007/s40314-019-0857-x

22. K. Iwata, C. Miyakoshi, A simulation on potential secondary spread of novel coronavirus in an exported country using a stochastic epidemic SEIR model, *J. Clin. Med.*, **9** (2020), 944. https://doi.org/10.3390/jcm9040944

23. P. Grandits, R. M. Kovacevic, V. M. Veliov, Optimal control and the value of information for a stochastic epidemiological SIS-model, *J. Math. Anal. Appl.*, **476** (2019), 665–695. https://doi.org/10.1016/j.jmaa.2019.04.005

24. A. Din, Y. Li, A. Yusuf, Delayed hepatitis B epidemic model with stochastic analysis, *Chaos Solitons Fract.*, **146** (2021), 110839. https://doi.org/10.1016/j.chaos.2021.110839

25. A. L. Krause, L. Kurowski, K. Yawar, R. A. Van Gorder, Stochastic epidemic metapopulation models on networks: SIS dynamics and control strategies, *J. Theor. Biol.*, **449** (2018), 35–52. https://doi.org/10.1016/j.jtbi.2018.04.023

26. L. J. Allen, E. J. Allen, A comparison of three different stochastic population models with regard to persistence time, *Theor. Popul. Biol.*, **64** (2003), 439–449. https://doi.org/10.1016/S0040-5809(03)00104-7

27. S. Okyere, J. A. Prah, A. N. O. Sarpong, An Optimal Control Model of the transmission dynamics of COVID-19 in Ghana, preprint paper, 2022. https://doi.org/10.48550/arXiv.2202.06413

28. P. Van den Driessche, J. Watmough, Reproduction numbers and sub-threshold endemic equilibria for compartmental models of disease transmission, *Math. Biosci.*, **180** (2002), 29–48. https://doi.org/10.1016/S0025-5564(02)00108-6

29. Z. Han, Q. Wang, H. Wu, Z. Hu, Stochastic P-bifurcation in a delayed Myc/E2F/miR-17-92 network, *Int. J. Bifurcat. Chaos*, **32** (2022), 2250159. https://doi.org/10.1142/S0218127422501590

30. X. Zhang, J. Fu, S. Hua, H. Liang, Z. K. Zhang, Complexity of Government response to COVID-19 pandemic: a perspective of coupled dynamics on information heterogeneity and epidemic outbreak, *Nonlinear Dynam.*, **2013** (2013), 1–20. https://doi.org/10.1007/s11071-023-08427-5

31. S. H. Oh, S. Y. Lee, C. Han, The effects of social media use on preventive behaviors during infectious disease outbreaks: the mediating role of self-relevant emotions and public risk perception, *Health Commun.*, **36** (2021), 972–981. https://doi.org/10.1080/10410236.2020.1724639

32. H. Huang, Y. Chen, Y. Ma, Modeling the competitive diffusions of rumor and knowledge and the impacts on epidemic spreading, *Appl. Math. Comput.*, **388** (2021), 125536. https://doi.org/10.1016/j.amc.2020.125536

33. D. H. Morris, F. W. Rossine, J. B. Plotkin, S. A. Levin, Optimal, near-optimal, and robust epidemic control, *Commun. Phys.*, **4** (2021), 78. https://doi.org/10.1038/s42005-021-00570-y

AIMS Press